



A new approach to solving multiorder time-fractional advection–diffusion–reaction equations using BEM and Chebyshev matrix

Moein Khalighi^{1,2} | Mohammad Amirianmatlob^{1,3} | Alaeddin Malek¹

¹Department of Applied Mathematics, Tarbiat Modares University, Tehran, Iran

²Department of Future Technologies, University of Turku, Turku, Finland

³Department of Mathematics and Statistics, Dalhousie University, Halifax, Canada

Correspondence

Moein Khalighi, Department of Applied Mathematics, Tarbiat Modares University, Tehran, Iran.

Email: moein.khalighi@utu.fi

Communicated by: Y. Zhou

Present Address

Moein Khalighi, Department of Future Technologies, Faculty of Sciences and Engineering, Yliopistonmaki, FI-20014, University of Turku, Finland.

In this paper, the boundary element method is combined with Chebyshev operational matrix technique to solve two-dimensional multiorder time-fractional partial differential equations: nonlinear and linear in respect to spatial and temporal variables, respectively. Fractional derivatives are estimated by Caputo sense. Boundary element method is used to convert the main problem into a system of a multiorder fractional ordinary differential equation. Then, the produced system is approximated by Chebyshev operational matrix technique, and its condition number is analyzed. Accuracy and efficiency of the proposed hybrid scheme are demonstrated by solving three different types of two-dimensional time-fractional convection–diffusion equations numerically. The convergent rates are calculated for different meshing within the boundary element technique. Numerical results are given by graphs and tables for solutions and different type of error norms.

KEYWORDS

boundary element method, Chebyshev operational matrix, multiorder fractional differential equations

MSC CLASSIFICATION

65N35; 65N38; 35R11

1 | INTRODUCTION

Fractional order differential operators are the representative of nonlocal phenomena, whereas many integer-order differential operators are mostly applied to examine local phenomena¹; therefore, fractional calculus can be useful to describe many of real-world problems that cannot be covered in the classic mathematical literature.^{2,3} Because the next state of many systems depends on its current and historical states, there is a great demand to improve topical methods for the real life problems.^{4,5} These problems happen in bioengineering,⁶ solid mechanics,⁷ anomalous transport,⁸ continuum and statistical mechanics,⁹ economics,¹⁰ relaxation electrochemistry,¹¹ diffusion procedures,¹² complex networks,^{13,14} and optimal control problems.^{15,16} Fractional diffusion equations are largely used in describing abnormal convection phenomenon of liquid in medium. Models of convection–diffusion quantities play significant roles in many practical applications,^{4,5} especially those involving fluid flow and heat transfer, such as thermal pollution in river system, leaching of salts in soils for computational simulations, oil reservoir simulations, transport of mass and energy, and global weather production. Numerical methods for convection–diffusion equations described by derivatives with inte-

This is an open access article under the terms of the Creative Commons Attribution License, which permits use, distribution and reproduction in any medium, provided the original work is properly cited.

© 2020 The Authors. *Mathematical Methods in the Applied Sciences* published by John Wiley & Sons Ltd.

ger order have been studied extensively.¹⁷ Due to the mathematical complexity, analytical solutions are very few and are restricted to the solution of simple fractional ordinary differential equations (ODEs).¹⁸ Several numerical techniques for solving fractional partial differential equations (PDEs) have been reported, such as variational iteration,¹⁹ Adomian decomposition,²⁰ operational matrix of B-spline functions,²¹ operational matrix of Jacobi polynomials,¹² Jacobi collocation,²² operational matrix of Chebyshev polynomials,^{23,24} Legendre collocation,²⁵ pseudo-spectral,²⁶ and operational matrix of Laguerre polynomials,²⁷ Pade approximation, and two-sided Laplace transformations.²⁸ Besides finite elements and finite differences,²⁹ spectral methods are one of the three main methodologies for solving various types of fractional differential equations.³⁰⁻³⁴ The main idea of spectral methods is to express the solution of differential equations as a sum of basis functions and then to choose the coefficients in order to minimize the error between the numerical and exact solutions as much as possible.³⁵ Therefore, high accuracy and ease of implementing are two of the main features that have encouraged many researchers to apply such methods to solve various types of fractional integral and differential equation. In this article, shifted chebyshev polynomials are used,³⁶ indeed it would be promising to apply spectral tau methods with other orthogonal polynomials, for example, Legendre³⁷ or Jacobi.³⁸

The boundary element method (BEM) always requires a fundamental solution to the original differential equation in order to avoid domain integrals in the formulation of the boundary integral equation. In addition, the nonhomogeneous and nonlinear terms are incorporated in the formulation by means of domain integrals. The basic idea of BEM is the transformation of the original differential equation into an equivalent integral equation only on the boundary, which has been widely applied in many areas of engineering such as fluid mechanics,³⁹ magnetohydrodynamic,⁴⁰ and electrodynamics.⁴¹

In this paper, the BEM is developed for the numerical solution of time-fractional partial differential equations (TFPDEs) for nonhomogeneous bodies, which converts the main problem into a system of fractional ODE with initial conditions, described by an equation having a known fundamental solution. The proposed method introduces an additional unknown domain function, which represents the fictitious source function for the equivalent problem. This function is determined from a supplementary domain integral equation, which is converted to a boundary integral equation using a meshless technique based on global approximation by a radial basis function (RBF) series.

The Delaunay graph mapping method can be viewed as a fast interpolation scheme. Despite its efficiency, the mesh quality for large deformation may deteriorate near the boundary, in particular, if the deformation involves large rotation, which may even lead to an invalid Delaunay graph. Furthermore, the RBF method can generally better preserve the mesh quality near the boundary, but the computational cost is much higher, as the mesh size increases. In order to develop methods that are more efficient and because of their flexibility and simplicity, the Delaunay graph-based RBF method (DG-RBF) were proposed⁴² to overcome the difficulty of meshing and remeshing the entire structure. Thus, the pure boundary character of the method is maintained, because elements discretization and the integrations are limited only to the boundary. To obtain the fictitious source, we use the Chebyshev spectral method based on operational matrix. The primary aim of this method is to propose a suitable way to approximate linear multiorder fractional ODEs with constant coefficients using a shifted Chebyshev Tau method that guarantees an exponential convergence speed.⁴³ Once the fictitious source is established, the solution of the original problem can be calculated from the integral representation of the solution in the substituted problem.

The outline of this paper is as follows. In Section 2, we introduce the multiorder time-fractional convection diffusion equation (TFCDE) for a class of the TFPDEs as a mathematical modeling of natural phenomena, and some basic preliminaries are also given. Section 3 is devoted to applying the BEM for converting the main problem into a system of multiorder fractional ODE with initial conditions. In Section 4, the Chebyshev operational matrix (COM) of fractional derivative is obtained by applying the spectral methods to solve the generated multiorder fractional ODE. In order to demonstrate the efficiency and accuracy of the proposed method, along with the analysis of the condition number of COM, some numerical experiments are presented in Section 6 using the definitions and lemmas of Section 5. Eventually, we conclude the paper with some remarks and add the appendix to make more convenient understanding of the proposed algorithm.

2 | PROBLEM STATEMENT

Assume that we are given the following initial boundary value problem for the multiorder time-fractional PDE in the two-dimensional domain Ω with boundary Γ ,

$$\sum_{j=0}^k \gamma_j(\mathbf{x}) D_c^{\alpha_j} u = A(\mathbf{x})u_{xx} + 2B(\mathbf{x})u_{xy} + C(\mathbf{x})u_{yy} + D(\mathbf{x})u_x + E(\mathbf{x})u_y + F(\mathbf{x})u + g(\mathbf{x}, t), \quad (1)$$

where $A(\mathbf{x})$, $B(\mathbf{x})$, $C(\mathbf{x})$, $D(\mathbf{x})$, $E(\mathbf{x})$, $F(\mathbf{x})$, and $\gamma_j(\mathbf{x})$ for $j = 0, 1, 2, \dots, k$ and $g(\mathbf{x}, t)$ are specified functions their physical meaning depends on that of the field function $u(\mathbf{x}, t)$, and

$$0 < \alpha_0 < \alpha_1 < \dots < \alpha_{k-1} < \alpha_k, \quad m - 1 < \alpha_k \leq m,$$

$$\mathbf{x} = (x, y) \in \Omega \cup \Gamma, \quad t > 0,$$

subject to the boundary conditions

$$B(u) = h(\mathbf{x}, t), \quad \mathbf{x} \in \Gamma, \quad (2)$$

and the initial conditions

$$D_c^i u(\mathbf{x}, 0) = d_i(\mathbf{x}), \quad i = 0, 1, \dots, m - 1 \quad (3)$$

in which m is an integer number and $D_c^\alpha u$ is the Caputo fractional time derivative of order α_j . The Caputo derivative,¹² is employed because initial conditions having direct physical meaning can be prescribed. This derivative is defined as

$$D_c^\alpha u(x, y, t) = \begin{cases} \frac{1}{\Gamma(m-\alpha)} \int_0^t \frac{u^{(m)}(x, y, \tau) d\tau}{(t-\tau)^{1+\alpha-m}}, & m - 1 < \alpha < m, \\ \frac{d^m}{dt^m} u(x, y, t), & \alpha = m \in \mathbb{N}. \end{cases} \quad (4)$$

$B(\cdot)$ is a linear operator with respect to spatial variables x, y of order one. $h(\mathbf{x}, t)$ and $d_i(\mathbf{x})$ ($i = 0, \dots, m - 1$) are specified functions in Equations (2) and (3), respectively. It seems that we could be able to recover the multiterm of classical diffusion equation for $\alpha_k = 1$, $\gamma_j(\mathbf{x}) = 0$ for $j = 0, \dots, k - 1$, $\gamma_k(\mathbf{x}) \neq 0$ and the classical wave equation in presence of viscous damping for $\alpha_k = 2$, $\alpha_{k-1} = 1$, $\gamma_k(\mathbf{x}) \neq 0$, $\gamma_{k-1}(\mathbf{x}) \neq 0$ and $\gamma_j(\mathbf{x}) = 0$ for $j = 0, \dots, k - 2$.

3 | IMPLEMENTATION OF BOUNDARY ELEMENT METHOD

Taking advantage of the following boundary element, the initial boundary value of the Equations (1–3) is reformed into an ODE problem.

Let $u(\mathbf{x}, t)$ be the sought solution to the problem (1–3) and assume that u is twice continuously differentiable in Ω . After applying Laplace operator on u , we have³⁹

$$\nabla^2 u(\mathbf{x}, t) = \mathfrak{B}(\mathbf{x}, t), \quad (5)$$

where $\mathfrak{B}(\mathbf{x}, t)$ known as an unknown fictitious source function. That is the solution of Equation (1) could be established by solving Equation (5) under the boundary condition (2), if convenient $\mathfrak{B}(\mathbf{x}, t)$ is first established. This is accomplished by adhering to the following procedure.

We write the solution of Equation (5) in the integral form. Thus, for u_n , as the normal derivative of u , we have⁴⁴

$$\varepsilon u(\mathbf{x}, t) = \int_{\Omega} u^* \mathfrak{B} d\Omega - \int_{\Gamma} (u^* u_n - u_n^* u) d\Gamma, \quad \mathbf{x} \in \Omega \cup \Gamma, \quad (6)$$

where $u^* = \ln r/2\pi$ is the fundamental solution to Equation (5), r is the distance between any two points, and also u_n^* stands for its normal derivative on the boundary. ε is the free term coefficient taking the values $\varepsilon = 1$ if $\mathbf{x} \in \Omega$, $\varepsilon = \theta/2\pi$ if $\mathbf{x} \in \Gamma$, otherwise $\varepsilon = 0$; θ is the interior angle between the tangents of boundary at point \mathbf{x} . $\varepsilon = 1/2$ for points where the boundary is smooth. After applying Equation (6), to boundary points by means of Greens second identity,⁴⁵ we yield the boundary integral equation

$$\frac{\theta}{2\pi} u(\mathbf{x}, t) = \sum_{j=1}^M b_j \left[\frac{1}{2} \hat{u}_j + \int_{\Gamma} (u^*(\hat{u}_n)_j - u_n^* \hat{u}_j) d\Gamma \right] - \int_{\Gamma} (u^* u_n - u_n^* u) d\Gamma, \quad \mathbf{x} \in \Gamma, \quad (7)$$

where \hat{u}_j is a certain solution of the equation

$$\nabla^2 \hat{u}_j = f_j, \quad j = 1, 2, \dots, M, \quad (8)$$

Also M is the number of interior points inside Ω . Here b_j are the coefficients that must be determined to satisfy

$$\mathfrak{B}(\mathbf{x}, t) = \sum_{j=1}^M b_j f_j,$$

where $f_j = f_j(r)$, $r = |\mathbf{x} - \mathbf{x}_j|$ is a set of radial basis approximating functions; \mathbf{x}_j are collocation points in Ω . The radial basis function method is used to map the nodes rather than that based on surface or volume ratios.⁴² The algorithm is set out in the following procedure. At first, we generate the Delaunay graph by using all the boundary nodes of the original mesh, and then we locate the mesh points in the graph, after that, we move the Delaunay graph according to the specified geometric motion/deformation, and the final step is mapping the mesh points in the new graph according to the RBF matrix and Delaunay triangle. Procedures before the last step are exactly the same as the original Delaunay graph mapping method;⁴⁶ hence, the details of these steps are skipped in this paper. The difference is in the last step, where the radial basis function interpolation is used to calculate the displacement of the internal mesh nodes from the given displacement of the Delaunay triangle nodes on the boundary, while the original Delaunay mapping method uses surface or volume ratios to calculate the displacement of inner nodes. Equation (7) is solved numerically by using the BEM. The boundary integrals in Equation (7) are approximated using N boundary nodal points. Here, $\varepsilon = 1/2$, as we ace the smooth boundary.

The domain integral can be evaluated when the fictitious source is estimated by a radial basis function series, and subsequently, it is reformed to a boundary line integral using the Green's reciprocal identity.⁴⁵ For the sake of simplification, we use multiquadric radial basis function in practice. M internal nodals are here used to define Delaunay linear triangular elements in Ω . Therefore, after discretization and application of the boundary integral Equation (7) at the N boundary nodal points, we have

$$\mathbf{H}\mathbf{u} = \mathbf{G}\mathbf{u}_n + \bar{\mathbf{A}}\mathbf{b}, \quad (9)$$

where \mathbf{H} and \mathbf{G} are $N \times N$ known as coefficient matrices originating from the integration of the kernel functions on the boundary elements and $\bar{\mathbf{A}}$ is an $N \times M$ coefficient matrix originating from the integration of the kernel function on the domain elements; \mathbf{u} and \mathbf{u}_n are vectors containing the nodal values of the boundary displacements and their normal derivatives. Also, \mathbf{b} is the vector of the nodal values of the fictitious source at the M internal nodal points.

For a second order differential equation, the boundary condition is a correlation of $\delta_1(\mathbf{x})\mathbf{u} + \delta_2(\mathbf{x})\mathbf{u}_n = h(\mathbf{x}, t)$; after applying it at the N boundary nodal points yields

$$\delta_1\mathbf{u} + \delta_2\mathbf{u}_n = \mathbf{h}(t), \quad (10)$$

where δ_1 and δ_2 are $N \times N$ known diagonal matrices and $\mathbf{h}(t) = [h(x_{BP_1}, t), \dots, h(x_{BP_N}, t)]^T$ is a known boundary vector, where x_{BP_j} are N boundary nodal points. Equations (9) and (10) can be combined and solved for \mathbf{u} and \mathbf{u}_n . This yields

$$\begin{aligned} \mathbf{u} &= [(\delta_1 + \delta_2\mathbf{G}^{-1}\mathbf{H})^{-1}(\delta_2\mathbf{G}^{-1}\mathbf{A})] \mathbf{b} + (\delta_1 + \delta_2\mathbf{G}^{-1}\mathbf{H})^{-1}\mathbf{h}(t), \\ \mathbf{u}_n &= [(\delta_1\mathbf{H}^{-1}\mathbf{G} + \delta_2)^{-1}(-\delta_1\mathbf{H}^{-1}\mathbf{A})] \mathbf{b} + (\delta_1\mathbf{H}^{-1}\mathbf{G} + \delta_2)^{-1}\mathbf{h}(t). \end{aligned} \quad (11)$$

Further, differentiating Equation (6) for points inside the domain ($\varepsilon = 1$) with respect to x and y , using the same discretization and collocating at the M internal nodal points, we have the following expression for the spatial derivatives

$$\hat{\mathbf{u}}_{pq} = \hat{\mathbf{H}}_{pq}\mathbf{u} + \hat{\mathbf{G}}_{pq}\mathbf{u}_n + \hat{\mathbf{A}}_{pq}\mathbf{b}, \quad p, q = 0, x, y \quad (12)$$

where the $\hat{\mathbf{u}}_{pq}$ is vector of values for u and its derivatives at the M internal nodal points; $\hat{\mathbf{H}}_{pq}$ and $\hat{\mathbf{G}}_{pq}$ are $M \times N$ known coefficient matrices originating from the integration of the kernel functions on the boundary elements and $\hat{\mathbf{A}}_{pq}$ is an $M \times M$ coefficient matrix originating from the integration of the kernel functions on the domain elements.

Eliminating \mathbf{u} and \mathbf{u}_n from Equation (12) using Equations (11) yields

$$\hat{\mathbf{u}}_{pq} = \mathbf{U}_{pq}\mathbf{b} + \mathbf{c}_{pq}, \quad p, q = 0, x, y \quad (13)$$

where

$$\begin{aligned} \mathbf{U}_{pq} &= \hat{\mathbf{H}}_{pq}(\delta_1 + \delta_2\mathbf{G}^{-1}\mathbf{H})^{-1}(\delta_2\mathbf{G}^{-1}\mathbf{A}) + \hat{\mathbf{G}}_{pq}(\delta_1\mathbf{H}^{-1}\mathbf{G} + \delta_2)^{-1}(-\delta_1\mathbf{H}^{-1}\mathbf{A}) + \hat{\mathbf{A}}_{pq}, \\ \mathbf{c}_{pq} &= [\hat{\mathbf{H}}_{pq}(\delta_1 + \delta_2\mathbf{G}^{-1}\mathbf{H})^{-1} + \hat{\mathbf{G}}_{pq}(\delta_1\mathbf{H}^{-1}\mathbf{G} + \delta_2)^{-1}] \mathbf{h}(t). \end{aligned} \quad (14)$$

The final step of the method is to apply Equation (1) at the M internal nodal points. This gives

$$\sum_{j=0}^k \gamma_j D_c^{\alpha_j} \hat{\mathbf{u}} = \mathbf{A}\hat{\mathbf{u}}_{xx} + 2\mathbf{B}\hat{\mathbf{u}}_{xy} + \mathbf{C}\hat{\mathbf{u}}_{yy} + \mathbf{D}\hat{\mathbf{u}}_x + \mathbf{E}\hat{\mathbf{u}}_y + \mathbf{F}\hat{\mathbf{u}} + \mathbf{g}(t), \quad (15)$$

where $\hat{\mathbf{u}} = \hat{\mathbf{u}}_{00}$ and γ_j , \mathbf{A} , \mathbf{B} , \mathbf{C} , \mathbf{D} , \mathbf{E} , and \mathbf{F} are $M \times M$ known diagonal matrices including the nodal values of the corresponding functions $\gamma_j(\mathbf{x})$, $A(\mathbf{x})$, $B(\mathbf{x})$, $C(\mathbf{x})$, $D(\mathbf{x})$, $E(\mathbf{x})$, and $F(\mathbf{x})$, respectively, and $\mathbf{g}(t) = [g(x_{IP_1}, t), \dots, g(x_{IP_M}, t)]^T$ is a known internal vector, where x_{IP_j} are M internal nodal points. Substituting the corresponding terms from Equation (13) into Equation (15) yields

$$\sum_{j=0}^k \mathbf{S}_j D_c^{\alpha_j} \mathbf{b}(t) = \mathbf{N}\mathbf{b}(t) + \mathbf{f}(t), \quad (16)$$

where

$$\begin{aligned} \mathbf{S}_j &= \gamma_j \mathbf{U}, \\ \mathbf{N} &= \mathbf{A}\mathbf{U}_{xx} + 2\mathbf{B}\mathbf{U}_{xy} + \mathbf{C}\mathbf{U}_{yy} + \mathbf{D}\mathbf{U}_x + \mathbf{E}\mathbf{U}_y + \mathbf{F}\mathbf{U}, \\ \mathbf{f}(t) &= \mathbf{A}\mathbf{c}_{xx} + 2\mathbf{B}\mathbf{c}_{xy} + \mathbf{C}\mathbf{c}_{yy} + \mathbf{D}\mathbf{c}_x + \mathbf{E}\mathbf{c}_y + \mathbf{F}\mathbf{c} + \mathbf{g}(t) - \sum_{j=0}^k \gamma_j D_c^{\alpha_j}(\mathbf{c}), \end{aligned} \quad (17)$$

in which $\mathbf{U} = \mathbf{U}_{00}$ and $\mathbf{c} = \mathbf{c}_{00}$ for $j = 0, \dots, k$. Now, from Equation (13), we can write the initial conditions (3) for $i = 0, 1, \dots, m-1$ in the form

$$\mathbf{b}^{(i)}(0) = \mathbf{U}^{-1} [\mathbf{d}_i - \mathbf{c}^{(i)}(0)], \quad (18)$$

where $\mathbf{d}_i(t) = [d_i(x_{IP_1}, t), \dots, d_i(x_{IP_M}, t)]^T$.

The above proposed procedure reduces the problem of multiorder two-dimensional time-fractional PDE (1–3) to a simpler system of multiterm fractional ODE (16) with initial condition (18). The existence, uniqueness, and continuous dependence of the system Equations (16–18) when $\mathbf{S}_k = \mathbf{1}$ can be rigorously discussed (see, e.g., Diethelm and Neville's paper⁴⁷). In the next section, we show the implementation of Chebyshev operational matrix, as a spectral technique³⁶ for fractional calculus, to solve the system of initial value problem (16–18).

4 | COM METHOD FOR SYSTEM OF MULTIORDER FRACTIONAL ODES

The Chebyshev polynomials $T_i(t)$ are defined on the interval $(-1, 1)$.⁴³ Thus, by changing variable $t \rightarrow \frac{2t}{L} - 1$, the shifted Chebyshev polynomials $T_{L,i}(t)$ of degree i on the interval $t \in (0, L)$, with an orthogonality relation can be introduced by^{36,48}

$$T_{L,i}(t) = i \sum_{j=0}^i (-1)^{i-j} \frac{(i+j-1)! 2^{2j}}{(i-j)!(2j)! L^j} t^j,$$

where $T_{L,i}(0) = (-1)^i$ and $T_{L,i}(L) = 1$. In this form, $T_{L,i}(t)$ may be generated by the following recurrence formula:

$$T_{L,i+1}(t) = 2(2t/L - 1)T_{L,i}(t) - T_{L,i-1}(t), \quad i = 1, 2, \dots \quad (19)$$

where $T_{L,0}(t) = 1$ and $T_{L,1}(t) = 2t/L - 1$. Therefore, a given function $f \in L^2[0, 1]$ may be approximated by $K + 1$ terms of shifted Chebyshev polynomials as

$$f(t) \simeq f_K(t) = \sum_{i=0}^K c_i T_{L,i}(t),$$

where the coefficients c_i are described by weight functions $w_L(t) = \frac{1}{\sqrt{Lt-t^2}}$ as $c_j = \frac{1}{h_i} \int_0^L f(t) T_{L,i}(t) w_L(t) dt$; in which $h_i = \pi$ for $i = 0$, otherwise $h_i = \frac{\pi}{2}$. If we set

$$\Phi(t) = [T_{L,0}(t), T_{L,1}(t), \dots, T_{L,K}(t)]^T \quad (20)$$

and suppose $\nu > 0$ and the ceiling function $\lceil \nu \rceil$ denotes the smallest integer greater than or equal to ν , then

$$D_c^\nu \Phi(t) \simeq \mathfrak{D}^{(\nu)} \Phi(t), \quad (21)$$

where $\mathfrak{D}^{(v)}$ is the $(K + 1) \times (K + 1)$ COM of derivatives of order v in the Caputo sense and is defined by^{36,48}

$$\mathfrak{D}^{(v)} = \begin{pmatrix} 0 & 0 & 0 & \dots & 0 \\ \vdots & \vdots & \vdots & \dots & \vdots \\ 0 & 0 & 0 & \dots & 0 \\ S_v([v], 0) & S_v([v], 1) & S_v([v], 2) & \dots & S_v([v], K) \\ \vdots & \vdots & \vdots & \dots & \vdots \\ S_v(i, 0) & S_v(i, 1) & S_v(i, 2) & \dots & S_v(i, K) \\ \vdots & \vdots & \vdots & \dots & \vdots \\ S_v(K, 0) & S_v(K, 1) & S_v(K, 2) & \dots & S_v(K, K) \end{pmatrix}, \quad (22)$$

where

$$S_v(i, j) = \sum_{\lambda=[v]}^i \frac{(-1)^{i-\lambda} 2i(i+\lambda-1)! \Gamma\left(\lambda-v+\frac{1}{2}\right)}{\rho_j L^v \Gamma\left(\lambda+\frac{1}{2}\right) (i-\lambda)! \Gamma(\lambda-v-j+1) \Gamma(\lambda+j-v+1)},$$

where $\rho_0 = 2$, $\rho_\lambda = 1$, $\lambda \geq 1$. Note that in $\mathfrak{D}^{(v)}$, the first $[v]$ rows are all zero. In order to solve Equation (16) with initial conditions (18), we approximate $\mathbf{b}(t)$ and $\mathbf{f}(t)$ in terms of shifted Chebyshev polynomials as

$$\mathbf{b}(t) = \begin{bmatrix} \sum_{i=0}^K \psi_i^1 T_{L,i}(t) \\ \vdots \\ \sum_{i=0}^K \psi_i^M T_{L,i}(t) \end{bmatrix} = \begin{bmatrix} \Psi^{1^T} \Phi(t) \\ \vdots \\ \Psi^{M^T} \Phi(t) \end{bmatrix} = \Psi \Phi(t), \quad (23)$$

$$\mathbf{f}(t) = \begin{bmatrix} \sum_{i=0}^K \ell_i^1 T_{L,i}(t) \\ \vdots \\ \sum_{i=0}^K \ell_i^M T_{L,i}(t) \end{bmatrix} = \begin{bmatrix} \omega^{1^T} \Phi(t) \\ \vdots \\ \omega^{M^T} \Phi(t) \end{bmatrix} = \omega \Phi(t), \quad (24)$$

where for $j = 1, \dots, M$

$$\Psi^{j^T} = [\psi_0^j, \dots, \psi_K^j],$$

$$\omega^{j^T} = [\ell_0^j, \dots, \ell_K^j],$$

and Ψ, ω are $M \times (K + 1)$ matrices that are defined as

$$\Psi = \begin{bmatrix} \Psi^{1^T} \\ \vdots \\ \Psi^{M^T} \end{bmatrix}, \quad \omega = \begin{bmatrix} \omega^{1^T} \\ \vdots \\ \omega^{M^T} \end{bmatrix}.$$

For $j = 0, \dots, k$, Equations (21) and (23) can be used to write

$$D_c^{\alpha_j} \mathbf{b}(t) \simeq \Psi D_c^{\alpha_j} \Phi(t) \simeq \Psi \mathfrak{D}^{(\alpha_j)} \Phi(t). \quad (25)$$

Employing Equations (23), (24), and (25), then the residual for Equation (16) can be written as

$$\mathbf{R}(t) = \left(\sum_{j=0}^k \mathbf{S}_j \Psi \mathfrak{D}^{(\alpha_j)} - \mathbf{N} \Psi - \omega \right) \Phi(t). \quad (26)$$

$\mathbf{R}(t)$ is a M vector with respect to t . If $R_j(t)$ be the j th component of $\mathbf{R}(t)$, then in a typical Tau method,⁴³ we generate $M(K - m + 1)$ linear equations with $M(K + 1)$ unknown coefficients of Ψ by applying

$$\langle R_i(t), T_{L,j}(t) \rangle = \int_0^L R_i(t) T_{L,j}(t) dt = 0, \quad i = 1, \dots, M, \quad j = 0, 1, \dots, K - m. \quad (27)$$

Also, by substituting Equation (23) into Equation (18), and with the fact that

$$\mathfrak{D}^{(n)} = (\mathfrak{D}^{(1)})^n, \quad n \in \mathbb{N},$$

we get a system of Mm linear equations with $M(K+1)$ unknown coefficients for Ψ as following

$$\mathbf{b}^{(i)}(0) = \Psi \mathfrak{D}^{(i)} \Phi(0) = \mathbf{U}^{-1} [\mathbf{d}_i - \mathbf{c}^{(i)}(0)], \quad i = 0, 1, \dots, m-1. \quad (28)$$

Equations (27) and (28) can be rewritten in the matrix form

$$\mathbf{A}\Psi = \mathbf{B}, \quad (29)$$

where \mathbf{A} is an $M(K+1) \times M(K+1)$ coefficient matrix. The system of algebraic Equations (29) can be easily solved for the unknown vector Ψ . Consequently, $\mathbf{b}(t)$ given in Equation (23) can be calculated, which gives a solution of Equation (16) with the initial conditions (18). Once the vector $\mathbf{b}(t)$ of the values of the fictitious source at the M internal nodal points has been established, then the solution of Equation (1) and its derivatives can be computed from Equation (13). For the points $\mathbf{x} = (x, y)$ that do not coincide with the prespecified internal nodal points, the solution could be drawn from the discretized counterpart of Equation (6) with $\varepsilon = 1$ using the same boundary and new domain discretization. Note that here the matrices $\hat{\mathbf{H}}_{pq}$, $\hat{\mathbf{G}}_{pq}$, and $\hat{\mathbf{A}}_{pq}$ corresponding to previous internal nodes plus the additional points must be recomputed.

5 | ERROR ESTIMATION

The convergence of the proposed method is shown by employing the following error norms, maximum error (L_∞), maximum relative error (MRE) to assess the accuracy of the method in multiscale problems and root mean square (RMS) to globally examine the method efficiency,

$$L_\infty = \max_{1 \leq i \leq M} |u_{\text{ex}}^i - u_{\text{app}}^i|, \quad (30)$$

$$MRE = \max_{1 \leq i \leq M} \left| \frac{u_{\text{ex}}^i - u_{\text{app}}^i}{u_{\text{ex}}^i} \right|, \quad (31)$$

$$RMS = \sqrt{\frac{1}{M} \sum_{i=1}^M (u_{\text{ex}}^i - u_{\text{app}}^i)^2}, \quad (32)$$

where u_{ex}^i and u_{app}^i denote the i th components of the exact and approximated solutions, respectively, and M denotes the number of internal points. It is not convenient to certainly determine what is the convergence rate of the proposed hybrid method; for example, for the number of nodal points N and M , and the size of the shifted Chebyshev polynomials K , the convergence order of the method would be $O(f(r^p, \tau^q))$, where f is a function of the convergence rate of BEM with the order p and the convergence rate of COM with the order q . The accuracy of the method depends on several factors, the convergence speed for BEM, the domain and boundary discretization, the shape parameters of radial basis functions, the orders of the derivatives, and condition number of COMs, as such the analysis of truncation errors for methods solving a two-dimensional multiterm time-fractional differential equation is not straightforward. Nonetheless, information about matrix \mathbf{A} from the algebraic system (29), particularly its condition number, will be useful. The condition number is defined by⁴³

$$\text{Cond}(\mathbf{A}) = \frac{\max\{|\lambda| : \det(\mathbf{A} - \lambda I) = 0\}}{\min\{|\lambda| : \det(\mathbf{A} - \lambda I) = 0\}},$$

such that a matrix with a large condition number is so-called *ill conditioned*, whereas the matrix is named *well conditioned* if its condition number is of a moderate size. We also suggest two P orders in the following lemmas to examine the rate of convergence for BEM and COM distinctly. The first one is directly tested by the exact solution and the effect of domain discretization, whereas the second one is addressed by comparing a sequence of numerical solutions of the ODE system (16) with different degree sizes of COMs that have been offered exponential rates of convergence accuracy for smooth problems in simple geometries.⁴³

Lemma 5.1. *Let the vector \mathbf{U} be the exact solution of the initial boundary value problem (1–3) and $\mathbf{u}_1, \mathbf{u}_2$ the approximate solutions with N_1, M_1 and N_2, M_2 of nodal points, respectively. Then, the computational order of the BEM method proposed*

in Section 3 can be calculated with P_r order $\simeq \log(E_{r_1}/E_{r_2})/\log(r_1/r_2)$ in which E_{r_1} and E_{r_2} are corresponded RMS errors (32) with the relative boundary mesh size $r_1 = 1/N_1$ and $r_2 = 1/N_2$, respectively.

Proof. When the leading terms in the spatial-discretization error are proportional to r_1^p and r_2^p , and $\|\cdot\|_{RMS}$ denoting the root mean square norm (32),

$$\|\mathbf{U} - \mathbf{u}_1\|_{RMS} = E_{r_1} = c_1 r_1^p \simeq c r_1^p, \quad \|\mathbf{U} - \mathbf{u}_2\|_{RMS} = E_{r_2} = c_2 r_2^p \simeq c r_2^p.$$

Hence,

$$\frac{E_{r_1}}{E_{r_2}} \simeq \frac{r_1^p}{r_2^p},$$

then taking logarithm from both sides yields

$$p \simeq \frac{\log\left(\frac{E_{r_1}}{E_{r_2}}\right)}{\log\left(\frac{r_1}{r_2}\right)}. \quad \square$$

Lemma 5.2. Let the vector \mathbf{b}_{ex} be the exact solution and $\mathbf{b}_1, \mathbf{b}_2$, and \mathbf{b}_3 be the approximate solutions of the multiterm fractional ODE (16) with the initial condition (18) at the same M fictitious source points using K_1, K_2 , and K_3 the numbers of shifted Chebyshev polynomials, respectively. With considering this proportion

$$\frac{K_1}{K_2} = \frac{K_2}{K_3}, \quad (33)$$

the temporal convergence order for the COM method presented in Section 4 is estimated using P_τ order $\simeq \log\left(\frac{\|\mathbf{b}_2 - \mathbf{b}_1\|_b}{\|\mathbf{b}_3 - \mathbf{b}_2\|_b}\right) / \log\left(\frac{\tau_1}{\tau_2}\right)$ in which the norm $\|\cdot\|_b$ define as $\|\mathbf{b}_s - \mathbf{b}_t\|_b = \sqrt{\frac{1}{M} \sum_{i=1}^M (b_s^i - b_t^i)^2}$, where b_s^i and b_t^i denote the i th components, and $\tau_1 = 1/K_1$, $\tau_2 = 1/K_2$, and $\tau_3 = 1/K_3$.

Proof. When the leading terms in the error of COM are proportional to τ_1^p , τ_2^p , and τ_3^p ,

$$\|\mathbf{b}_{ex} - \mathbf{b}_1\|_b = c'_1 \tau_1^p \simeq c' \tau_1^p, \quad \|\mathbf{b}_{ex} - \mathbf{b}_2\|_b = c'_2 \tau_2^p \simeq c' \tau_2^p, \quad \|\mathbf{b}_{ex} - \mathbf{b}_3\|_b = c'_3 \tau_3^p \simeq c' \tau_3^p,$$

thus

$$\mathbf{b}_{ex} \simeq \frac{\|\tau_2^p \mathbf{b}_1 - \tau_1^p \mathbf{b}_2\|_b}{\tau_2^p - \tau_1^p}, \quad \mathbf{b}_{ex} \simeq \frac{\|\tau_3^p \mathbf{b}_2 - \tau_2^p \mathbf{b}_3\|_b}{\tau_3^p - \tau_2^p},$$

according to Equation (33), we have

$$\frac{\|\mathbf{b}_2 - \mathbf{b}_1\|_b}{\|\mathbf{b}_3 - \mathbf{b}_2\|_b} \simeq \left(\frac{\tau_1}{\tau_2}\right)^p.$$

Hence,

$$p \simeq \frac{\log\left(\frac{\|\mathbf{b}_2 - \mathbf{b}_1\|_b}{\|\mathbf{b}_3 - \mathbf{b}_2\|_b}\right)}{\log\left(\frac{\tau_1}{\tau_2}\right)}. \quad \square$$

In the following section, the numerical errors are computed based on assumptions described in Lemmas 5.1 and 5.2.

6 | NUMERICAL RESULTS AND DISCUSSION

On the basis of the described procedure, some problems are solved to illustrate the efficiency and the accuracy of the proposed method. In the first example, a simple two-dimensional fractional heat-like equation is considered for two different conditions. In the second example, a nonlinear two-dimensional fractional wave-like equation is tested. In the third and fourth problems, two linear TFCDEs are solved to test the impact of external force (g) and the final time on the convergence

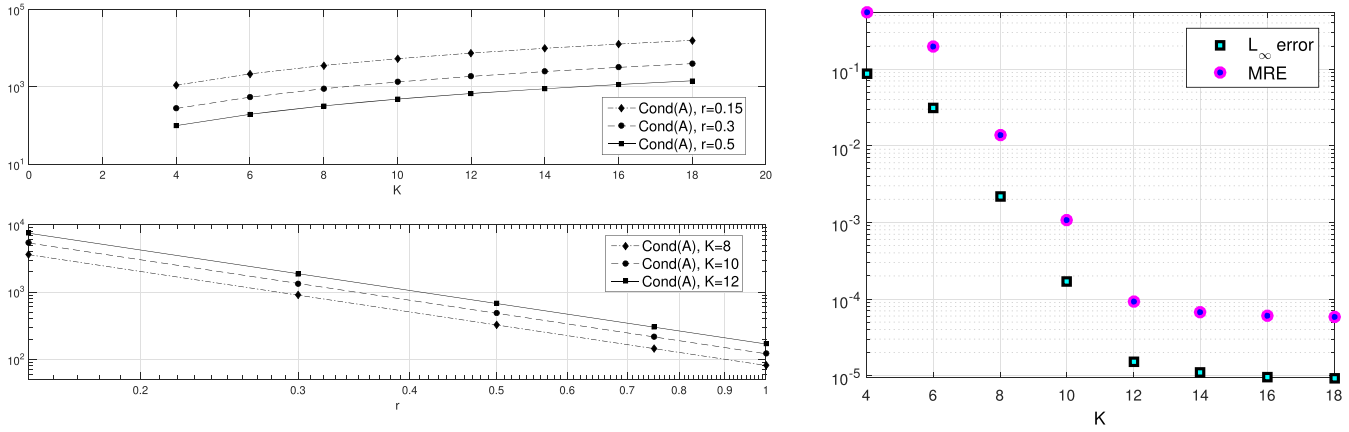


FIGURE 1 The location of nodal points and relative distances for constant element discretization [Colour figure can be viewed at wileyonlinelibrary.com]

rate of the method. In the fifth and sixth test problems, multiorder time-fractional diffusion-wave equations in bounded homogeneous anisotropic plane bodies are solved. The condition number of system 29 is examined for each example. Because the size of the matrix \mathbf{A} depends on the number of internal points, M , and the degree of COM, K , the condition number of \mathbf{A} can be compared versus K and the length of distance between nodal points. However, most domains are not discretized uniformly. In this regard, suppose r denotes the mean length of all the distances between the internal points and their adjacent points (e.g., see x_{IP} in Figure 1). Thus, the numerical results show that the condition number behaves as $Cond\mathbf{A} \simeq r^{-2}(K + 1)^2$ for Example 6.1 and $Cond\mathbf{A} \simeq r^{-2}(K + 1)^3$ for other examples.

Example 6.1. Consider the following two-dimensional time-fractional heat-like equation:

$$D_c^\alpha u = u_{xx} + u_{yy}, \quad 0 < \alpha \leq 1, \quad t > 0$$

subjected to different initial conditions with different domains^{49,50}:

$$(I) \quad u(x, y, 0) = \sin x \sin y, \quad 0 < x, y < 2\pi, \quad (II) \quad u(x, y, 0) = \cos\left(\frac{\pi}{2}x\right) \cos\left(\frac{\pi}{2}y\right), \quad 0 < x, y < 1,$$

Here, boundary conditions satisfy the exact solutions:

$$(I) \quad u(x, y, t) = E_\alpha(-2t^\alpha) \sin x \sin y, \quad (II) \quad u(x, y, t) = E_\alpha\left(-\frac{1}{2}\pi^2 t^\alpha\right) \cos\left(\frac{\pi}{2}x\right) \cos\left(\frac{\pi}{2}y\right), \quad (34)$$

where the following one-parameter Mittag-Leffler function is defined as

$$E_\alpha(z) = \sum_{k=0}^{\infty} \frac{z^k}{\Gamma(\alpha k + 1)}, \quad \alpha > 0.$$

Figure 2 demonstrates L_∞ errors and MRE versus the degree K (right) for Example 6.1 (case I) when $N = 160$ and $\alpha = 0.5$ at $t = 1.5$. The convergence rate of COM is estimated that P_r order > 5 . Furthermore, the condition numbers of \mathbf{A} , on the Figure 2 (left), are shown versus the polynomial degree, K , and the mean length of discrete elements, r . It can be numerically deduced that the condition number behaves as $Cond(\mathbf{A}) \simeq r^{-2}(K + 1)^2$; for example, when $K = 8$, then $Cond(\mathbf{A}) \simeq 76.4 \times r^{-2}$, and when $r = 0.3$, then $Cond(\mathbf{A}) \simeq 10.43 \times K^2$. In Table 1, numerical results are compared with the exact solutions (34) for Example 6.1, case I, for fixed $K = 12$, $t = 1.5$, with the differential orders $\alpha = 0.5$ and $\alpha = 0.75$, and different number of nodal points; the convergence rate of BEM is algebraic (P_r order > 4.4) when the number of nodal points is increased from $N = 40$ to $N = 80$ and it is quadratic (P_r order > 2) when $N = 80$ goes to $N = 160$. Apart from the value of α , it can be inferred that the computation cost of the second discretization for moderate N and M is more effective

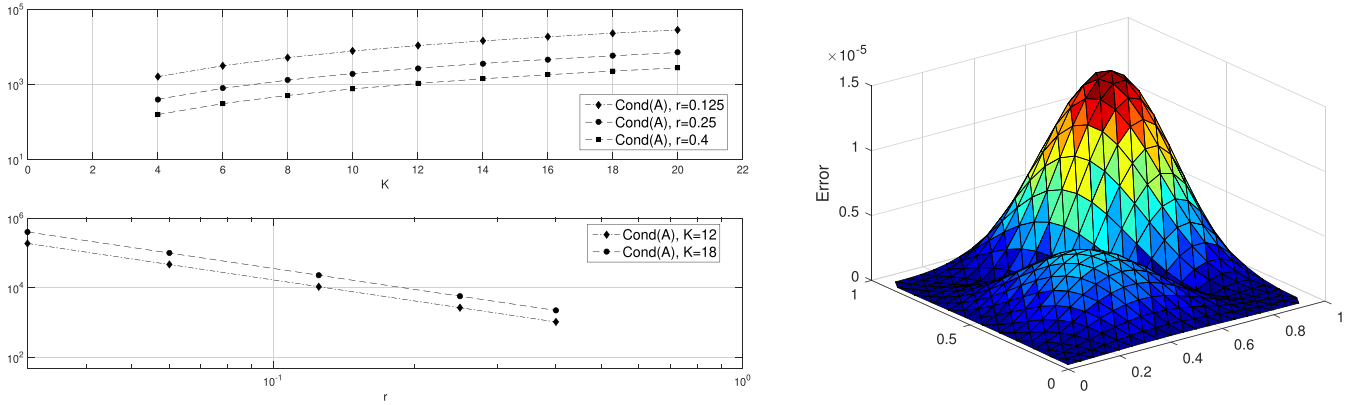


FIGURE 2 The condition number of A versus the polynomial degree K and the mean length of discrete elements r (left) and a comparison of L_∞ errors and MRE versus K (right) at $t = 1.5$ when $N = 160$ and $\alpha = 0.5$ for Example 6.1 case I ; P_r order = 5.13 is estimated for $K = 4, 8, 16$ [Colour figure can be viewed at wileyonlinelibrary.com]

FIGURE 3 The condition number of A versus the polynomial degree K and the mean length of discrete elements r (left) and the relative absolute errors (right) obtained for Example 6.1 case II when $N = 200$, $K = 12$, $\alpha = 0.5$, and $t = 0.5$ [Colour figure can be viewed at wileyonlinelibrary.com]

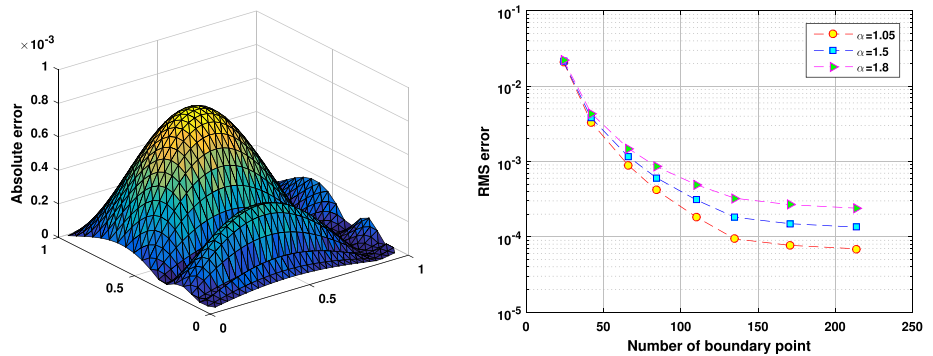


TABLE 1 The error norms and the estimated order of convergence P_r for the vector solution \mathbf{U} according to the Lemma 5.1, in Example 6.1 case I when $K = 12$ and $t = 1.5$

N	$\alpha = 0.5$			$\alpha = 0.75$		
	MRE	RMS	P_r order	MRE	RMS	P_r order
40	5.48066×10^{-3}	2.38289×10^{-4}	—	8.21377×10^{-3}	3.57120×10^{-4}	—
80	2.52922×10^{-4}	1.09966×10^{-5}	4.4376	3.72158×10^{-4}	1.61807×10^{-5}	4.4641
160	6.10497×10^{-5}	2.65433×10^{-6}	2.0506	8.43489×10^{-5}	3.66734×10^{-6}	2.1415

than the third one. For case (II) , a similar behavior of $Cond(A)$ versus K and r is shown in Figure 3 (left). The relative absolute error (right) with $N = 200$, and $K = 12$ for the final time $t = 1$ is exhibited. Intuitively, the relative absolute errors are approached to 10^{-5} , which it could be expected for $K = 12$ and $N = 200$ based on the information from Table 2. This table shows the estimated convergence for two terms of shifted Chebyshev series for the final time $t = 0.5$; in general, there is an improvement for errors when the degree K increases, but no relationship between P_r order and degree K is observed. It may also be concluded $N = 64$ is more computational cost-effective in this case.

Example 6.2. Consider the two-dimensional time-fractional wave-like equation⁵¹:

$$D_t^\alpha u = \frac{1}{12} (x^2 u_{xx} + y^2 u_{yy}), \quad 0 < x, y < 1, \quad 1 < \alpha \leq 2, \quad t > 0,$$

subjected to boundary conditions

$$\begin{aligned} u(0, y, t) = 0, & \quad u(1, y, t) = 4 \cosh t, \\ u(x, 0, t) = 0, & \quad u(x, 1, t) = 4 \sinh t, \end{aligned}$$

and the initial condition

$$\begin{aligned} u(\mathbf{x}, 0) &= x^4, \\ u'(\mathbf{x}, 0) &= y^4. \end{aligned}$$

N	K = 12			K = 18		
	L_∞	RMS	P_r order	L_∞	RMS	P_r order
8	1.9970×10^{-3}	1.8930×10^{-3}	–	1.3222×10^{-3}	1.0553×10^{-3}	–
16	1.4673×10^{-3}	7.1121×10^{-4}	1.4123	1.0571×10^{-3}	5.1238×10^{-4}	1.0424
32	6.0501×10^{-4}	1.2220×10^{-4}	2.5410	3.5453×10^{-4}	7.1607×10^{-5}	2.8390
64	9.3468×10^{-5}	9.9095×10^{-6}	3.6243	6.9059×10^{-5}	7.3216×10^{-6}	3.2899
128	3.8455×10^{-5}	1.8098×10^{-6}	2.4530	2.4404×10^{-5}	1.1486×10^{-6}	2.6723

TABLE 2 A comparison of the error norms and the estimated order of convergence P_r for the vector solution \mathbf{U} according to the Lemma 5.1, in Example 6.1 case II for two fixed K

K	L_∞	MRE	RMS	$\ \mathbf{b}_i - \mathbf{b}_{i-1}\ _b$	P_r order	Cond(A)
8	7.15174×10^{-3}	2.25751×10^{-2}	2.91855×10^{-3}	–	–	4.54024×10^5
16	2.82029×10^{-5}	8.43598×10^{-5}	1.06609×10^{-5}	5.5885×10^{-6}	–	2.96189×10^6
32	1.07633×10^{-5}	2.08835×10^{-5}	6.63201×10^{-6}	5.0329×10^{-7}	3.4730	2.14632×10^7
64	8.17112×10^{-6}	5.69019×10^{-6}	9.87053×10^{-7}	3.2380×10^{-8}	3.9582	1.71381×10^8

TABLE 3 The error norms for the vector solution \mathbf{U} and the convergence orders of the vector solution \mathbf{b} in Example 6.2 for $\alpha = 2, N = 100$ and $t = 0.5$

The exact solution for $\alpha = 2$ is found to be

$$u(x, y, t) = x^4 \cosh t + y^4 \sinh t. \tag{35}$$

This problem is solved for different K with $N = 100$ at $t = 0.5$ and integer order $\alpha = 2$ to compare with the exact solution (35). The results from Table 3 offer an error improvement by increasing the number of degree K of COMs. The condition numbers of the system (29) illustrate such behavior $Cond(\mathbf{A}) \approx r^{-2}(K + 1)^3$ (see Table 3). Due to the fact that the domain and boundary nodal points are fixed here, the numerical solutions of \mathbf{U} are directly affected by the numerical solutions of \mathbf{b} ; in other words, affected by the accuracy of COM. However, the exact solution of the generated ODE system is not clear, and the convergence order of COMs is estimated by norm $\|\cdot\|_b$ for three distinct degrees with a same proportion. Interestingly, a comparison between the two columns RMS and $\|\cdot\|_b$ of Table 3 suggests direct relationships but with different speed between the approximation solution of \mathbf{U} and \mathbf{b} . In addition, by considering the scale of the solutions, and a comprehensive assessment of the absolute errors for distinct degrees K , it could be concluded that the Chebyshev Tau method converges with an oscillating manner around the exact solution of fractional ODE system (16).

Example 6.3. Consider the following TFCDE⁵²:

$$D_c^\alpha u = u_{xx} + u_{yy} - 5u_x - 5u_y + g(x, y, t),$$

$$1 < \alpha \leq 2, \quad (x, y) \in \Omega,$$

with the boundary condition and initial conditions

$$u(x, y, t) = 0, \quad (x, y) \in \Gamma, \quad 0 < t \leq 1,$$

$$u(x, y, 0) = 0, \quad \psi(x, y) = 0, \quad (x, y) \in \Omega,$$

where $\Omega = [0, 1]^2$. Then we have the following exact solution:

$$u(x, y, t) = 2^{12} t^{2+\alpha} x^3 (1-x)^3 y^3 (1-y)^3.$$

It is easy to check

$$g(x, y, t) = 2^{11} \Gamma(\alpha + 3) x^3 (1-x)^3 y^3 (1-y)^3 t^2$$

$$- 2^{12} (6x - 51x^2 + 120x^3 - 150x^4 + 30x^5) y^3 (1-y)^3 t^{2+\alpha}$$

$$- 2^{12} x^3 (1-x)^3 (6y - 51y^2 + 120y^3 - 105y^4 + 30y^5) t^{2+\alpha}.$$

This problem is challenging and sensitive because of the large numbers included in the function g . However, it could be compensated by multiplying to power functions of decimal numbers, and considering the final time $t = 1$. Figure 4 (left plan) shows the estimated error ranged around 10^{-4} , for $\alpha = 1.5$ and final time $t = 1$, with the degree $K = 10$, and (right plan) demonstrates the plot of the error versus the number of boundary nodes, N , with $K = 10$ for three different values α , illustrating that the smoothness roughly occurred after $N = 135$. The behavior of the condition number matrix \mathbf{A} is estimated as $Cond(\mathbf{A}) \approx r^{-2}(K + 1)^3$. Table 4 gives $Cond(\mathbf{A})$, the RMS error and the convergence rates are obtained by

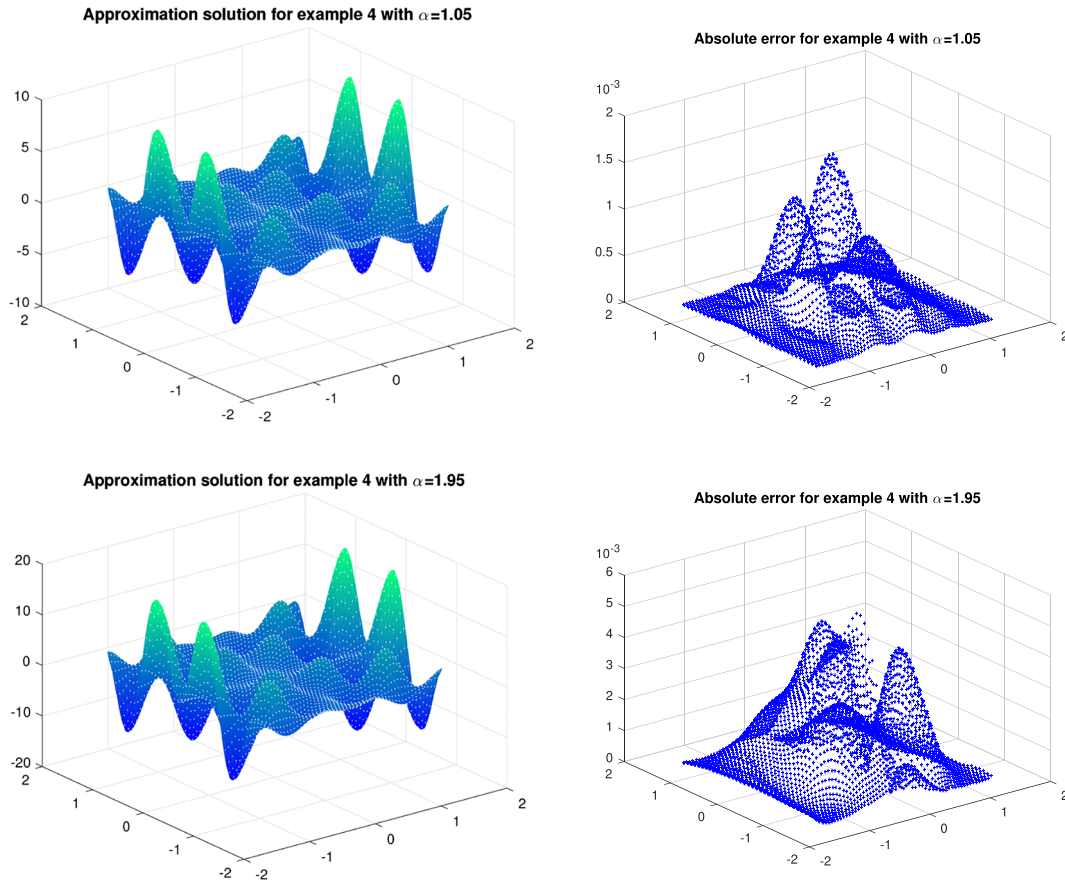


FIGURE 4 Graphs of the absolute error with $\alpha = 1.5$ and $K = 10$ (left) and a comparison of errors for different values of α (right) at finite time $t = 1$ for Example 6.3. [Colour figure can be viewed at wileyonlinelibrary.com]

TABLE 4 The RMS error of the vector solution \mathbf{U} and the convergence rate of COM and spatial-discretization base on Lemmas 5.1 and 5.2 for Example 6.3 at time $t = 1$

$K=16$			$\alpha=1.9$			$\alpha=1.1$			
N	RMS	$Cond(\mathbf{A})$	P_r order	RMS	$Cond(\mathbf{A})$	P_r order	RMS	$Cond(\mathbf{A})$	P_r order
40	8.8704×10^{-3}	4.86686×10^5	—	7.3330×10^{-3}	4.89036×10^5	—			
80	2.0840×10^{-3}	1.95421×10^6	2.0897	1.6591×10^{-3}	1.96064×10^6	2.1439			
160	4.8292×10^{-4}	7.78881×10^6	2.1095	3.5514×10^{-4}	7.80051×10^6	2.2240			
320	8.1966×10^{-5}	3.13058×10^7	2.5587	7.2452×10^{-5}	3.13134×10^7	2.2933			
$N=200$			$\alpha=1.9$			$\alpha=1.6$			
K	RMS	$\ \mathbf{b}_i - \mathbf{b}_{i-1}\ _b$	P_r order	RMS	$\ \mathbf{b}_i - \mathbf{b}_{i-1}\ _b$	P_r order	RMS	$\ \mathbf{b}_i - \mathbf{b}_{i-1}\ _b$	P_r order
10	1.3010×10^{-4}	—	—	7.5314×10^{-5}	—	—			
20	4.2187×10^{-5}	1.3840×10^{-6}	—	1.6938×10^{-5}	1.4839×10^{-6}	—			
40	1.2781×10^{-5}	3.7002×10^{-7}	1.9032	3.8515×10^{-6}	2.8012×10^{-7}	2.4053			
80	3.7745×10^{-6}	9.8207×10^{-8}	1.9137	8.8808×10^{-7}	4.8922×10^{-8}	2.5175			

solving Example 6.3 for different values of α . It indicates better RMS errors for α near to 1 than 2, that is not true for P_r orders.

Example 6.4. Consider the linear TFCDE⁵³:

$$D_c^\alpha u = u_{xx} + u_{yy} - 0.1u_x - 0.1u_y + g(x, y, t),$$

$$1 < \alpha \leq 2, \quad (x, y) \in \Omega,$$

with the initial conditions

$$u(x, y, 0) = 0, \quad u'(x, y, 0) = 0, \quad (x, y) \in \Omega,$$

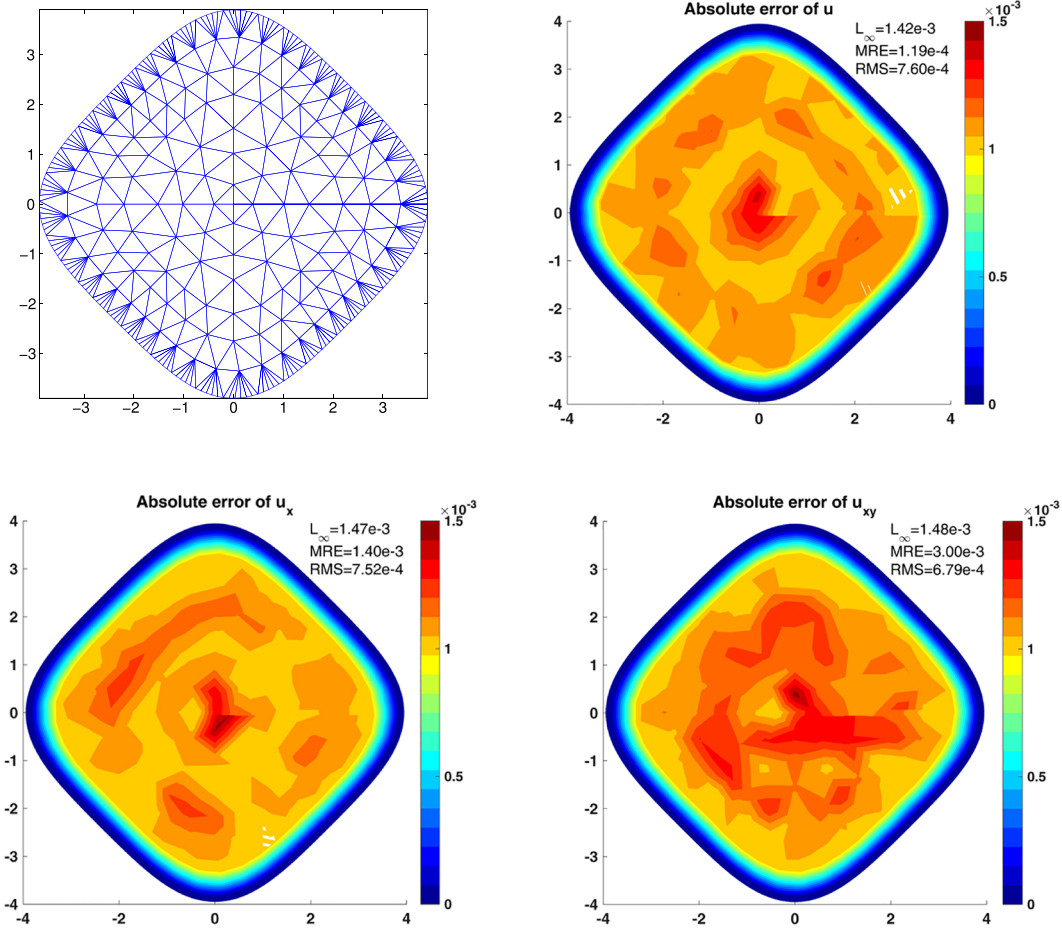


FIGURE 5 Graphs of approximation solution and the absolute error obtained for Example 6.4 for $\alpha = 1.05$ and $\alpha = 1.95$ with $K = 10$ and $N = 255$ for final time $t = 2$ [Colour figure can be viewed at wileyonlinelibrary.com]

RMS – error				
N	$\alpha = 1.1$	$\alpha = 1.4$	$\alpha = 1.7$	$\alpha = 1.9$
10	1.5030×10^{-1}	1.0628×10^{-1}	1.2802×10^{-1}	1.1669×10^{-1}
20	3.5223×10^{-2}	3.8318×10^{-2}	5.0480×10^{-2}	4.7404×10^{-2}
40	1.6236×10^{-2}	1.1808×10^{-2}	1.4409×10^{-2}	1.1033×10^{-2}
80	2.4654×10^{-3}	4.9065×10^{-3}	2.0146×10^{-3}	4.5839×10^{-3}
160	1.2483×10^{-3}	9.5059×10^{-4}	9.5252×10^{-4}	1.1706×10^{-3}
320	3.7848×10^{-4}	2.0804×10^{-4}	1.7544×10^{-4}	2.1400×10^{-4}

TABLE 5 The RMS error for the vector solution \mathbf{U} , in Example 6.4 for $K = 8$ and $t = 2$

and the Dirichlet boundary conditions. The exact solution of the current test problem is

$$u(x, y, t) = t^{3+\alpha} \sin\left(\frac{\pi}{6}x\right) \sin\left(\frac{7\pi}{4}x\right) \sin\left(\frac{3\pi}{4}y\right) \sin\left(\frac{5\pi}{4}y\right),$$

where Ω is the computational domain as shown in Figure 5 (left plan). The approximate solution and its relative absolute error are shown in Figure 5 for $\alpha = 1.05$ and $\alpha = 1.95$ with $K = 10$ and $N = 255$ for the final time $t = 2$. Although $N = 255$ is considered to depict clear data points in the figure, $N = 150$ would be sufficient to achieve the semiequivalent errors. Importantly, by considering the results of the previous example 6.3 and Figure 5 (right plan), it may convey that the method has a better performance for the less values of α . In contrast, Table 5 refuses this idea; there are irrelevant outcomes versus the values of α , although the table shows a reliable numerical convergence.

Example 6.5. The multiorder time-fractional diffusion-wave equation⁴⁴

FIGURE 6 The geometry of the plane body discretization with $N = 210$, $M = 132$ with DG-RBF technique and contour plots of absolute errors when $K = 16$ for Example 6.5 [Colour figure can be viewed at wileyonlinelibrary.com]

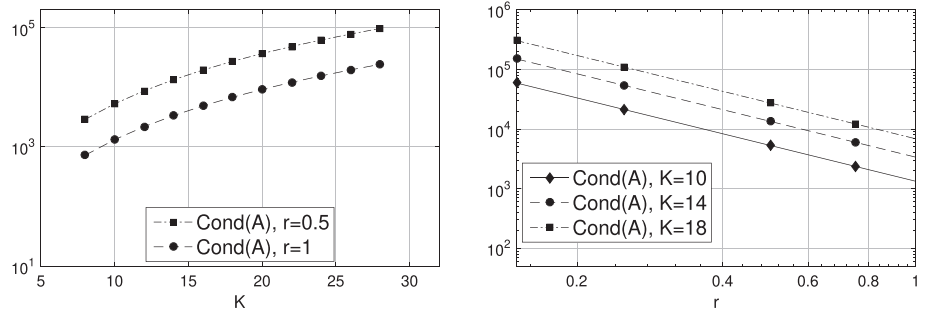


TABLE 6 The condition number of A , the RMS error, and the convergent order for the vector solution \mathbf{b} according to the Lemma 5.2 in Example 6.5 for $K = 16$ and $t = 4$

N	RMS – error			P_r order	$r \simeq$	$Cond(A)$
	u	u_x	u_{xy}			
50	6.27668×10^{-2}	6.69339×10^{-2}	6.37693×10^{-2}	–	2.4	8.5723×10^2
100	6.74090×10^{-3}	5.97502×10^{-3}	6.03444×10^{-3}	3.40157	1.2	3.4289×10^3
120	3.70614×10^{-3}	3.60496×10^{-3}	3.86762×10^{-3}	2.43988	0.1	4.9376×10^3
200	7.71852×10^{-4}	7.85751×10^{-4}	7.03289×10^{-4}	3.33700	0.6	1.3715×10^4

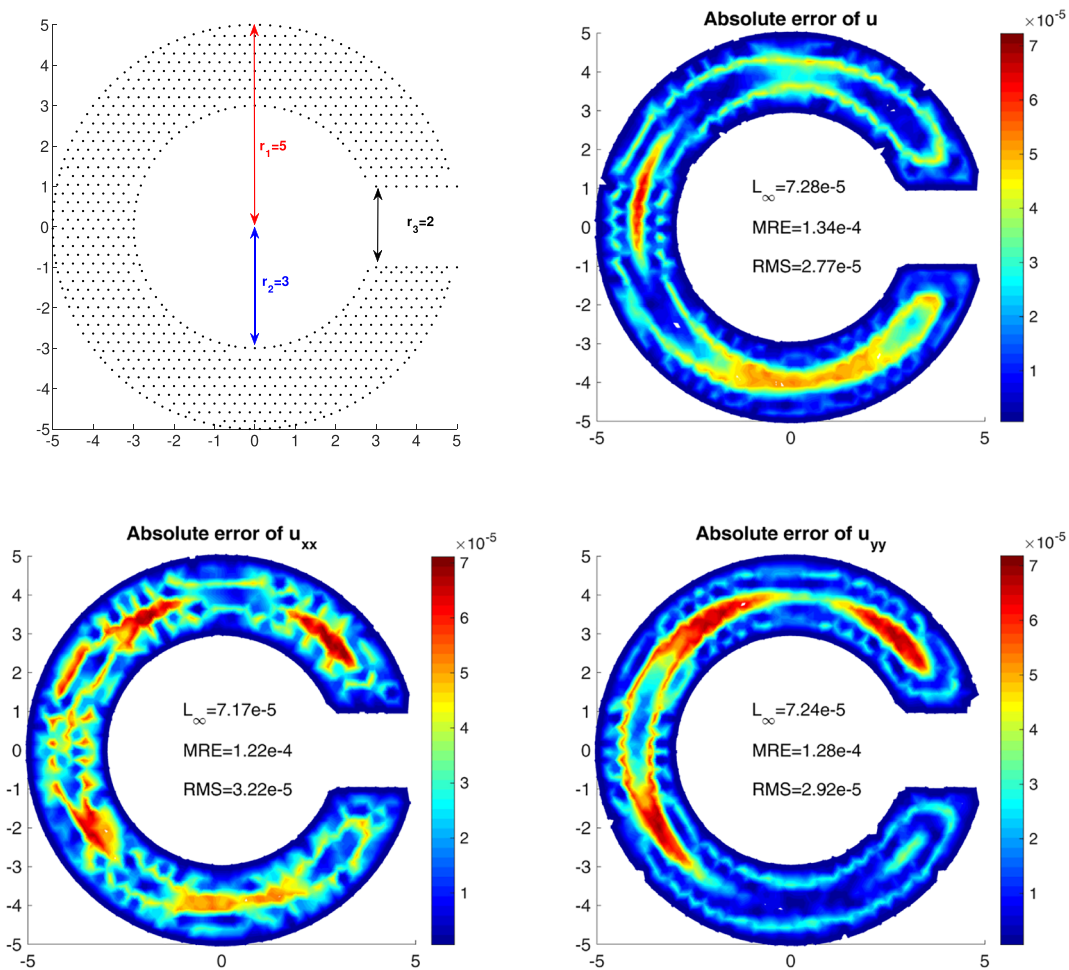


FIGURE 7 The condition number of matrix A versus the polynomial degree K (left) and versus the mean length of discrete element edges r (right) for Example 6.6 when $t = 5$

$$\gamma_1 D_c^{1.7} u + \gamma_0 D_c^{0.8} u = Au_{xx} + 2Bu_{xy} + Cu_{yy} + g(\mathbf{x}, t), \quad \mathbf{x}(x, y) \in \Omega, \quad t > 0, \quad (36)$$

in the plane inhomogeneous anisotropic body that is shown in Figure 6 has been solved, subject to boundary conditions

$$u(\mathbf{x}, t) = 0, \quad \mathbf{x}(x, y) \in \Gamma,$$

and the initial condition

$$\begin{aligned} u(\mathbf{x}, 0) &= 0, \\ u'(\mathbf{x}, 0) &= U(x, y), \end{aligned}$$

where $A = \frac{(y^2 - x^2 + 50)}{50}$, $B = \frac{2xy}{50}$, $C = \frac{(x^2 - y^2 + 50)}{50}$, $\gamma_1 = 5e^{(-0.1(|x|+|y|))}$, $\gamma_0 = 0.4(x^2 + y^2)^{1/2}$. The external source g is $g(\mathbf{x}, t) = U(\gamma_1 D_c^{1.7} T + \gamma_0 D_c^{0.8} T) - T(AU_{xx} + 2BU_{xy} + CU_{yy})$, where $U(x, y) = a^2 b^2 - \left(\left(\frac{x}{a} \right)^2 + \left(\frac{y}{b} \right)^2 \right) \left(\left(\frac{x}{b} \right)^2 + \left(\frac{y}{a} \right)^2 \right)$ and $T(t) = t - \frac{t^3}{6} + \frac{t^5}{200}$. The boundary of the domain is defined by the curve:

$$\Gamma = \frac{(ab)^{1/2}}{\left(\left(\cos \frac{\theta}{a} \right)^2 + \left(\sin \frac{\theta}{b} \right)^2 \right)^{(1/4)} \left(\left(\cos \frac{\theta}{b} \right)^2 + \left(\sin \frac{\theta}{a} \right)^2 \right)^{(1/4)},$$

where $0 \leq \theta \leq 2\pi$, $a = 3$, $b = 1.3$. The problem admits an exact solution $u_{exact} = T(t)U(x, y)$. This problem is solved using BEM and COM for various M and N when $K = 16$ at $t = 4$. The value of u , u_x , and u_{xy} are compared with the exact solution. Numerical results are given in Table 6 showing the efficiency of the proposed method by P_r order > 2 , and the condition number of matrix \mathbf{A} with the manner as $r^{-2} \times (K + 1)^3$. In Figure 6, the contour plots illustrate the absolute errors distributions of the approximations of u , u_x , and u_{xy} on the plane, including L_∞ , MRE , RMS , at $t = 4$ for specific nodal points and Delaunay triangulation when $N = 210$, $M = 132$, $K = 16$.

Example 6.6. Consider the large terms time-fractional diffusion equation

$$\sum_{j=0}^6 \gamma_j(\mathbf{x}) D_c^{\alpha_j} u = D(\mathbf{x})u_x + E(\mathbf{x})u_y + F(\mathbf{x})u + g(\mathbf{x}, t), \quad \mathbf{x}(x, y) \in \Omega, \quad t > 0, \quad (37)$$

in a 'C-shape' made by the elimination of a circle with radius $r_2 = 3$ and null origin from the inside of a circle with radius $r_1 = 5$ and the same origin, and extracting the space between the lines $y = -1$ and $y = 1$ from the right side of the outcome (see Figure A1) with the Dirichlet boundary conditions, and the initial condition

$$\begin{aligned} u(\mathbf{x}, 0) &= 0, \\ u'(\mathbf{x}, 0) &= U(\mathbf{x}), \end{aligned}$$

where $U(\mathbf{x}) = \cos(x)e^{\sin(y)}$ and the external force g is $g(\mathbf{x}, t) = U\bar{T} - T(DU_x + EU_y + FU)$ such that $T(t) = \frac{t^3}{6} - t$, and with the order of the derivatives $\alpha_6 = \frac{5}{3}$, $\alpha_5 = \frac{7}{5}$, $\alpha_4 = \frac{4}{3}$, $\alpha_3 = \frac{6}{5}$, $\alpha_2 = \frac{3}{2}$, $\alpha_1 = \frac{2}{3}$, and $\alpha_0 = \frac{1}{2}$, and their coefficients $\gamma_6 = \Gamma\left(\frac{1}{3}\right)$, $\gamma_5 = 4\pi$, $\gamma_4 = 2\pi$, $\gamma_3 = 4\pi$, $\gamma_2 = \sqrt{\pi}$, $\gamma_1 = \frac{\Gamma\left(\frac{1}{3}\right)}{3}$, $\gamma_0 = \frac{\sqrt{\pi}}{2}$, $D = \frac{r_2^2 - x^2}{r_1^2 - y^2}$, $E = \frac{x^2 - y^2}{r_1 - r_2}$, and $F = \sqrt{x^2 + y^2} + r_3$, we can set

$$\begin{aligned} \bar{T}(t) &= t^{\frac{5}{3}} \left(\frac{2\pi}{\Gamma\left(\frac{8}{3}\right)} + \frac{\Gamma\left(\frac{1}{3}\right)}{3\Gamma\left(\frac{11}{3}\right)} t \right) + t^{\frac{3}{2}} \left(\frac{20 - 8t}{15} \right) + t \left(\frac{9}{4} t^{\frac{1}{3}} + \frac{4\pi}{\Gamma\left(\frac{13}{5}\right)} t^{\frac{3}{5}} + \frac{4\pi t^{\frac{4}{5}}}{\Gamma\left(\frac{14}{5}\right)} \right) \\ &- \left(t^{-\frac{2}{3}} + t^{\frac{1}{3}} + t^{\frac{1}{2}} + t^{\frac{-1}{2}} + \sqrt{3}\Gamma\left(\frac{1}{3}\right) t^{-\frac{1}{3}} + \left(\sqrt{10 + 2\sqrt{5}} \right) \Gamma\left(\frac{2}{5}\right) t^{-\frac{2}{5}} + \left(\sqrt{10 - 2\sqrt{5}} \right) \Gamma\left(\frac{1}{5}\right) t^{-\frac{1}{5}} \right) \end{aligned}$$

to find the exact solution as $u_{exact} = T(t)U(\mathbf{x})$. This problem is solved with $N = 216$, $M = 741$, and $K = 16$, for $t = 5$. In Figure 7, the distribution of the absolute errors on the domain, L_∞ , MRE , and RMS of u , u_{xx} , and u_{yy} are illustrated. Figure 6 exhibits the behavior of the condition number matrix A as $r^{-2} \times (K+1)^3$; for example, when $r = 1$, $Cond(\mathbf{A}) \simeq 0.92 \times (K+1)^3$, and when $K = 10$, $Cond(\mathbf{A}) \simeq 1202.46 \times r^{-2}$. Among these six exams, an interesting point can be concluded that the error distribution into a plan depends not only on the positions of the nodal points but also on the final time solving the problem; with an increasingly asymmetric discretization, and longer computing time, the error distribution becomes more 'random'.

7 | CONCLUSION

Here, we have proposed a hybrid algorithm to solve two-dimensional multiorder time-fractional partial differential equations. Their general form is given in Equations (1–3). The method consists of the boundary element method combined with spectral Chebyshev operational matrix. The BEM is used to transfer the corresponding time-fractional PDE into a system of ODEs, whereas COM is used to solve the system efficiently. This method is applied to the two-dimensional fractional heat-like, wave-like, and diffusion-wave equations, which shows that the errors of the approximate solution decay exponentially. When the exact solution exists, comparison is made with $\|\mathbf{U}_{ex} - \mathbf{u}_{app}\|$, and the convergence rate is calculated using Lemma 5.1. When the exact solution is not in hand, the order of convergence is estimated by three approximate solutions with various degrees of Chebyshev polynomials in a same grid-point based on Lemma 5.2. By applying the assumptions of the Lemmas, the numerical results show the efficiency and convergence rate for the proposed hybrid method. Notwithstanding, it is not easy to emphasize a unique conclusion for the accuracy of the method on the ground that given the vast range of architectures, spectral methods, boundary element methods, fractional calculus, and meshing used with in such a hybrid-technique framework. In general, for multiorder two-dimensional time-fractional PDE (1–3), the current method calculate \mathbf{U} for the test exams, with this range of convergence rate: $2 < P_r \text{ order} < 4.5$ for the moderate values of N and M . And for multiterm fractional ODE (16) with initial condition (18), the current method works well to calculate solution \mathbf{b} with a range of the convergence rate around $1 < P_r \text{ order} < 5.5$. Moreover, The condition number of matrix \mathbf{A} from linear system (29) behaves like $Cond\mathbf{A} \simeq r^{-2}(K+1)^2$ for the problems with $[\alpha] = 1$, and $Cond\mathbf{A} \simeq r^{-2}(K+1)^3$ for the problems with $[\alpha] = 2$. For the future direction, the authors believe that establishing new methods to examine long-term effects of memory in complex systems modeled by fractional calculus is highly required as fractional calculus is a proper mathematical tool for describing memory,¹⁴ although the proposed COM technique is not an appropriate scheme for long-term problems. It is instead efficient for problems with multiterm orders.

ACKNOWLEDGEMENT

The authors are very grateful to the referees for carefully reading the paper and for their comments and suggestions which have improved the paper.

8 | CONFLICT OF INTEREST

The authors declare no conflict of interest.

REFERENCES

1. Teodoro GS, Machado JAT, De Oliveira EC. A review of definitions of fractional derivatives and other operators. *J Comput Phys*. 2019;388:195-208.
2. Metzler R, Klafter J. The random walk's guide to anomalous diffusion: a fractional dynamics approach. *Phys Reports*. 2000;339(1):1-77.
3. Matlob MA, Jamali Y. The concepts and applications of fractional order differential calculus in modeling of viscoelastic systems: a primer. *Crit Rev Biomed Eng*. 2019;47(4).
4. Sun HG, Zhang Y, Baleanu D, Chen W, Chen YQ. A new collection of real world applications of fractional calculus in science and engineering. *Commun Nonlinear Sci Numer Simul*. 2018;64:213-231.
5. Almeida R, Bastos NR, Monteiro MTT. Modeling some real phenomena by fractional differential equations. *Math Methods Appl Sci*. 2016;39(16):4846-4855.
6. Magin RL. *Fractional calculus in bioengineering* Begell House Redding; 2006.
7. Rossikhin YA, Shitikova MV. Applications of fractional calculus to dynamic problems of linear and nonlinear hereditary mechanics of solids. *Appl Mech Rev*. 1997;50(1):15-67.
8. Metzler R, Klafter J. The restaurant at the end of the random walk: recent developments in the description of anomalous transport by fractional dynamics. *J Phys A: Math Gen*. 2004;37(31):R161.
9. Mainardi F. *Fractional Calculus*: Springer; 1997;291-348.
10. Baillie RT. Long memory processes and fractional integration in econometrics. *J Econ*. 1996;73(1):5-59.
11. Oldham KB. Fractional differential equations in electrochemistry. *Adv Eng Softw*. 2010;41(1):9-12.
12. Podlubny I. *Fractional Differential Equations: An Introduction to Fractional Derivatives, Fractional Differential Equations, to Methods of Their Solution and Some of Their Applications* Elsevier; 1998.
13. Safdari H, Kamali MZ, Shirazi A, Khalighi M, Jafari G, Ausloos M. Fractional dynamics of network growth constrained by aging node interactions. *PLOS one*. 2016;11(5):e0154983.
14. Saeedian M, Khalighi M, Azimi-Tafreshi N, Jafari GR, Ausloos M. Memory effects on epidemic evolution: the susceptible-infected-recovered epidemic model. *Phys Rev E*. 2017;95(2):022409.
15. Zeid SS, Kamyad AV, Effati S, Rakhshan SA, Hosseinpour S. Numerical solutions for solving a class of fractional optimal control problems via fixed-point approach. *SeMA J*. 2017;74(4):585-603.
16. Hosseinpour S, Nazemi A. A collocation method via block-pulse functions for solving delay fractional optimal control problems. *IMA J Math Control Info*. 2016;34(4):1215-1237.
17. Heidari H, Malek A. Null boundary controllability for hyperdiffusion equation. *Internat J Appl Math*. 2009;22:615-626.
18. Kilbas AAA, Srivastava HM, Trujillo JJ. *Theory and Applications of Fractional Differential Equations*: Elsevier Science Limited; 2006.
19. Dehghan M, Yousefi SA, Lotfi A. The use of He's variational iteration method for solving the telegraph and fractional telegraph equations. *Int J Numer Methods Biomed Eng*. 2011;27(2):219-231.
20. Ford NJ, Connolly JA. Systems-based decomposition schemes for the approximate solution of multi-term fractional differential equations. *J Comput Appl Math*. 2009;229(2):382-391.
21. Lakestani M, Dehghan M, Irandoust-Pakchin S. The construction of operational matrix of fractional derivatives using B-spline functions. *Commun Nonlinear Sci Numer Sim*. 2012;17(3):1149-1162.
22. Lin Y, Xu Ch. Finite difference/spectral approximations for the time-fractional diffusion equation. *J Comput Phys*. 2007;225(2):1533-1552.
23. Taher AHS, Malek A, Momeni-Masuleh SH. Chebyshev differentiation matrices for efficient computation of the eigenvalues of fourth-order Sturm–Liouville problems. *Appl Math Model*. 2013;37(7):4634-4642.
24. Bhrawy AH, Alofi AS. The operational matrix of fractional integration for shifted Chebyshev polynomials. *Appl Math Lett*. 2013;26(1):25-31.
25. Mokhtary P. Reconstruction of exponentially rate of convergence to Legendre collocation solution of a class of fractional integro-differential equations. *J Comput Appl Math*. 2015;279:145-158.
26. Esmaeili S, Shamsi M. A pseudo-spectral scheme for the approximate solution of a family of fractional differential equations. *Commun Nonlinear Sci Numer Sim*. 2011;16(9):3646-3654.
27. Abdelkawy MA, Taha TM. An operational matrix of fractional derivatives of Laguerre polynomials. *Walailak J Sci Technol(WJST)*. 2014;11(12):1041-1055.
28. Hosseinpour S, Nazemi A, Tohidi E. A new approach for solving a class of delay fractional partial differential equations. *Mediterranean J Math*. 2018;15(6):218.
29. Li Ch, Zeng F. Finite difference methods for fractional differential equations. *Int J Bifurcation Chaos*. 2012;22(04):1230014.
30. Bhrawy AH, Zaky MA. Numerical simulation for two-dimensional variable-order fractional nonlinear cable equation. *Nonlinear Dyn*. 2015;80(1-2):101-116.

31. Bhrawy AH, Zaky MA, Van Gorder RA. A space-time Legendre spectral tau method for the two-sided space-time Caputo fractional diffusion-wave equation. *Numer Algorithms*. 2016;71(1):151-180.
32. Zaky MA, Hendy AS, Macías-Díaz JE. Semi-implicit Galerkin–Legendre spectral schemes for nonlinear time-space fractional diffusion–reaction equations with smooth and nonsmooth solutions. *J Sci Comput*. 2020;82(1):1-27.
33. Zaky MA, Machado JT. Multi-dimensional spectral tau methods for distributed-order fractional diffusion equations. *Comput Math Appl*. 2020;79(2):476-488.
34. Hafez RM, Zaky MA. High-order continuous Galerkin methods for multi-dimensional advection–reaction–diffusion problems. *Eng Comput*:1-17.
35. Zaky MA. A Legendre spectral quadrature tau method for the multi-term time-fractional diffusion equations. *Comput Appl Math*. 2018;37(3):3525-3538.
36. Bhrawy AH, Taha TM, Machado JAT. A review of operational matrices and spectral techniques for fractional calculus. *Nonlinear Dyn*. 2015;81(3):1023-1052.
37. Zaky MA. An improved tau method for the multi-dimensional fractional Rayleigh–Stokes problem for a heated generalized second grade fluid. *Comput Math Appl*. 2018;75(7):2243-2258.
38. Bhrawy AH, Zaky MA. A method based on the Jacobi tau approximation for solving multi-term time–space fractional partial differential equations. *J Comput Phys*. 2015;281:876-895.
39. Katsikadelis JT. *The Boundary Element Method for Engineers and Scientists: Theory and Applications* Academic Press; 2016.
40. Morovati V, Malek A. Solving inhomogeneous magnetohydrodynamic flow equations in an infinite region using boundary element method. *Eng Anal Bound Elem*. 2015;58:202-221.
41. Brebbia CA, Walker S. *Boundary Element Techniques in Engineering*. Elsevier; 2016.
42. Wang Y, Qin N, Zhao N. Delaunay graph and radial basis function for fast quality mesh deformation. *J Comput Phys*. 2015;294:149-172.
43. Canuto C, Hussaini MY, Quarteroni A, et al. *Spectral Methods in Fluid Dynamics*: Springer Science & Business Media; 2012.
44. Katsikadelis JT. The BEM for numerical solution of partial fractional differential equations. *Comput Math Appl*. 2011;62(3):891-901.
45. Katsikadelis JT. The BEM for nonhomogeneous bodies. *Archive Appl Mech*. 2005;74(11-12):780-789.
46. Liu X, Qin N, Xia H. Fast dynamic grid deformation based on Delaunay graph mapping. *J Comput Phys*. 2006;211(2):405-423.
47. Diethelm K, Ford NJ. Multi-order fractional differential equations and their numerical solution. *Appl Math Comput*. 2004;154(3):621-640.
48. Doha EH, Bhrawy AH, Ezz-Eldien SS. A Chebyshev spectral method based on operational matrix for initial and boundary value problems of fractional order. *Comput Math Appl*. 2011;62(5):2364-2373.
49. Momani S. Analytical approximate solution for fractional heat-like and wave-like equations with variable coefficients using the decomposition method. *Appl Math Comput*. 2005;165(2):459-472.
50. Shirzadi A, Ling L, Abbasbandy S. Meshless simulations of the two-dimensional fractional-time convection–diffusion–reaction equations. *Eng Anal Bound Elem*. 2012;36(11):1522-1527.
51. Shou DH, method HEJH. Beyond Adomian The variational iteration method for solving heat-like and wave-like equations with variable coefficients. *Phys Lett A*. 2008;372(3):233-237.
52. Wang Z, Vong S. *Comput Math Appl*. 2014;68(3):185-196.
53. Dehghan M, Safarpour M. The dual reciprocity boundary elements method for the linear and nonlinear two-dimensional time-fractional partial differential equations. *Math Method Appl Sci*. 2016;39(14):3979-3995.

How to cite this article: Khalighi M, Amirianmatlob M, Malek A. A new approach to solving multiorder time-fractional advection–diffusion–reaction equations using BEM and Chebyshev matrix. *Math Meth Appl Sci*. 2020;1–21. <https://doi.org/10.1002/mma.6352>

APPENDIX A: ALGORITHM IN A NUTSHELL

For convenience, a brief description of the proposed algorithm is given in this section.

At the beginning, determine N boundary points and divide M internal nodal points into groups by the Delaunay graph, then use the RBF method to interpolate the nodal points to its new position. Hence, there is no need to optimize shape parameters for the domain discretization. After discretization, consider \int_k indicating integration on k element on the boundary (see Figure A1 and Table A1) and set $i, k = 1, \dots, N, j = 1, \dots, M$ for the boundary points x_{BP_i} , the domain points x_{IP_j} , and the algorithm implementation. Notice that different θ must be considered for computing the boundary integrals at the corner points, particularly in inhomogeneous shapes, in comparing to smooth boundary.³⁹

Algorithm

- Step 0:** Input $M, N, r_{ik}, r_{jk}, f_j(r), \alpha = \{\alpha_0, \dots, \alpha_k\}$.
Implementation of boundary element method
- Step 1:** Initialize $\mathbf{u}^*, \mathbf{u}_n^*, \hat{\mathbf{u}}, \hat{\mathbf{u}}_n, \mathbf{A}, \mathbf{B}, \mathbf{C}, \mathbf{D}, \mathbf{E}, \mathbf{F}, \gamma_j, \mathbf{h}, \delta_1, \delta_2, \mathbf{d}$.
- Step 2:** Compute $\mathbf{H} = \tilde{\mathbf{H}} - \frac{\theta}{2\pi} \mathbf{I}$, where \mathbf{I} is an $N \times N$ identity matrix, and $\tilde{\mathbf{H}}(i, k) = \int_k \mathbf{u}_n^*(r_{ik}) ds$.
- Step 3:** Compute $\mathbf{G}(i, k) = \int_k \mathbf{u}^*(r_{ik}) ds$.
- Step 4:** Compute $\bar{\mathbf{A}}(i, k) = \frac{1}{2} \hat{\mathbf{u}}(r_{ji}) - \sum_{k=1}^N \tilde{\mathbf{H}}(i, k) \hat{\mathbf{u}}(r_{jk}) + \sum_{k=1}^N \mathbf{G}(i, k) \hat{\mathbf{u}}_n(r_{jk})$.
- Step 5:** Compute $\hat{\mathbf{H}}_{pq}(i, k) = \int_k (\mathbf{u}_n^*)_{pq}(r_{ik}) ds$, where $p, q = 0, x, y$.
- Step 6:** Compute $\hat{\mathbf{G}}_{pq}(i, k) = \int_k (\mathbf{u}^*)_{pq}(r_{ik}) ds$.
- Step 7:** Compute $\bar{\mathbf{A}}(i, k) = \frac{1}{2} \hat{\mathbf{u}}(r_{ji}) - \sum_{k=1}^N \tilde{\mathbf{H}}(i, k) \hat{\mathbf{u}}(r_{jk}) + \sum_{k=1}^N \mathbf{G}(i, k) \hat{\mathbf{u}}_n(r_{jk})$.
- Step 8:** Construct \mathbf{U}_{pq} and \mathbf{c}_{pq} by (14), consequently, \mathbf{S}, \mathbf{N} , and $\mathbf{f}(t)$ by (17).
Solving linear multi-order fractional ODE
- Step 9:** Construct vector function $\Phi(t)$ by (20) and (19), and spectral matrix $\mathfrak{D}^{(v)}$ for $v \in \alpha$ by (22).
- Step 10:** Construct vector function $\mathbf{R}(t)$ by (26).
- Step 11:** Construct $M(K + 1)$ linear system by solving (27) and using (28).
- Step 12:** Solve the generated algebraic system (29) for the vector Ψ .
- Step 13:** Compute unknown vector $\mathbf{b}(t)$ from (23).
- Step 14:** Output the corresponding solution of the problem (1) and its derivatives by applying equation (13).

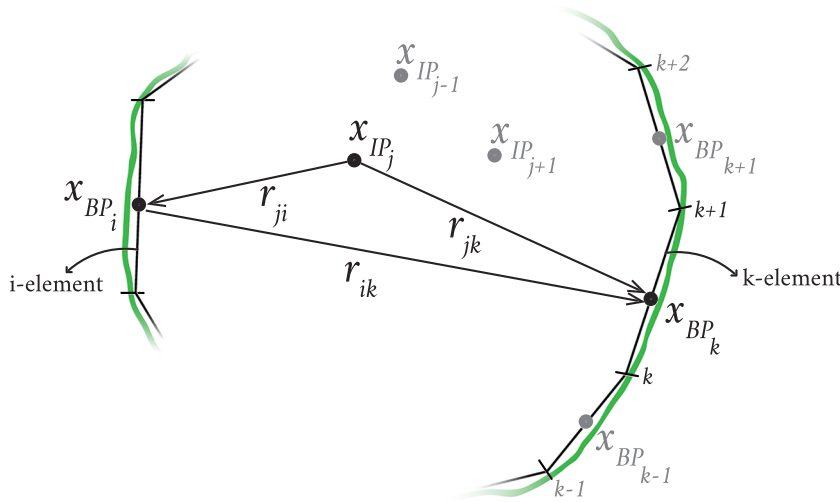


FIGURE A1 The geometry of the plane body discretization with $N = 216, M = 741$ with DG-RBF technique and contour plots of absolute errors when $K = 16$ for Example 6.6 [Colour figure can be viewed at wileyonlinelibrary.com]

TABLE A1 Notations and abbreviations used in this paper

Notation	Description
ODE	Ordinary differential equation
PDE	Partial differential equation
BEM	Boundary element method
TFPDE	Time-fractional PDE
TFCDE	Time-fractional convection–diffusion equation
COM	Chebyshev operational matrix
RBF	Radial basis function
DG-RBF	Delaunay graph-based RBF method
Ω	Two-dimensional domain
Γ	Two-dimensional boundary
$D_c^{\alpha_j}$	Caputo fractional time derivative of order α_j
$u(\mathbf{x}, t)$	Unknown field function of spatial $\mathbf{x} \in \Omega \cup \Gamma$ and time t
u_n	Normal derivative of u
$A, B, C,$	Given coefficient functions of \mathbf{x} and $j = 0, 1, \dots, k$
D, E, F, γ_j	
g	Given independent function of \mathbf{x} and t
B	Linear operator with respect to \mathbf{x} of order one
$h(\mathbf{x}, t)$	Given function in the boundary condition; $\mathbf{x} \in \Gamma$
$d_i(\mathbf{x})$	Given function in the initial condition; $i = 0, 1, \dots, m - 1$
$\mathfrak{B}(\mathbf{x}, t)$	Unknown fictitious source function
u^*, u_n^*	Fundamental solution of Equation (5), and normal derivative of u^* on the boundary
\hat{u}, \hat{u}_n	Particular solution of Equation (9), and normal derivative of \hat{u}
ε	Free term coefficient; $\varepsilon = 1$ if $\mathbf{x} \in \Omega$, $\varepsilon = \theta/2\pi$ if $\mathbf{x} \in \Gamma$, else $\varepsilon = 0$, see details in book ³⁹
θ	Interior angle between the tangents of boundary at point \mathbf{x} , see details in book ³⁹
r	Distance between two points (or mean of all distances of internal points)
M	Number of interior points after discretization
x_{IP_j}	M internal nodal points; $j = 1, \dots, M$
N	Number of boundary nodal points after discretization
x_{BP_j}	N boundary nodal points; $j = 1, \dots, N$
$f_j(r)$	Radial basis approximating functions, $j = 1, 2, \dots, M$

Continued

TABLE A1 Continues

Notation	Description
H, G	$N \times N$ known coefficient matrices from the integration of the kernel functions on the boundary
A	$N \times M$ known coefficient matrix from the integration of the kernel function on the domain
u, u_n	Unknown vectors of the nodal values of the boundary displacements and their normal derivatives
b(t)	Vector of the nodal values of the fictitious source at the M internal nodal points
δ_1, δ_2	$N \times N$ known diagonal matrices
h(t)	Known boundary vector of $h(x_{BP_j}, t), j = 1, \dots, N$
u_{pq}	Vector of values for u and its derivatives at the M internal nodal points; $\hat{\mathbf{u}}_{00} = \hat{\mathbf{u}}$
H_{pq}, G_{pq}	$M \times N$ known coefficient matrices from the integration of the kernel functions on the boundary
A_{pq}	$M \times M$ known coefficient matrix from the integration of the kernel functions on the domain
A, B, C,	$M \times M$ known diagonal matrices including the nodal values of the corresponding functions $A(\mathbf{x}), B(\mathbf{x}), C(\mathbf{x}), D(\mathbf{x}), E(\mathbf{x}), F(\mathbf{x}), \gamma_j(\mathbf{x})$
D, E, F, γ_j	
g(t)	Known internal vector of $g(x_{IP_j}, t), j = 1, \dots, M$
$T_{L,i}(t)$	Shifted Chebyshev polynomials of degree i on the interval $t \in (0, L)$
$\mathfrak{D}^{(v)}$	$(K + 1) \times (K + 1)$ Chebychev operational matrix of derivatives of order v in the sense of Caputo
Ψ	$M \times (K + 1)$ unknown matrix
ω	$M \times (K + 1)$ known matrix
R(t)	Residual vector of Equation (16) with length M
L_∞	Maximum error
MRE	Maximum relative error
RMS	Root mean square
P_r order	Convergence order of BEM approximated by the Lemma 5.1
P_r order	Convergence order of COM approximated by the Lemma 5.2
Cond(A)	Condition number of matrix A of the algebraic system Equations 29